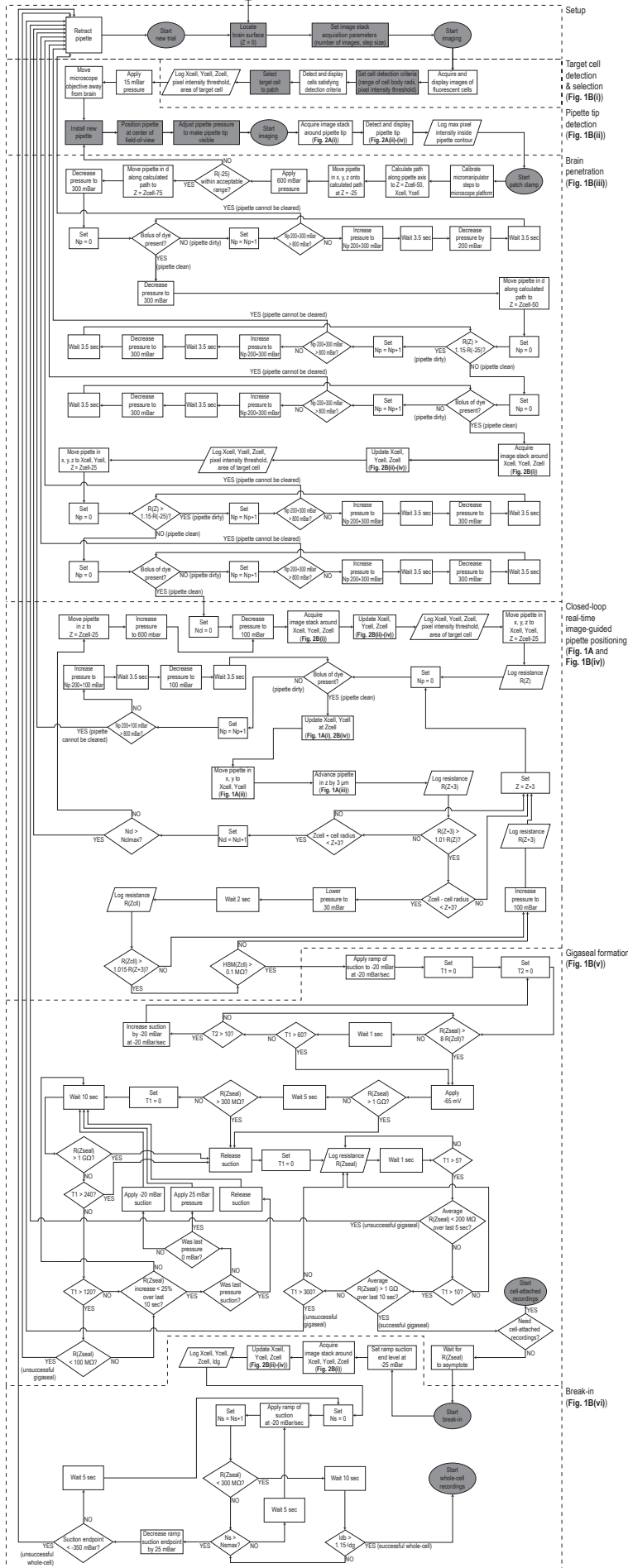
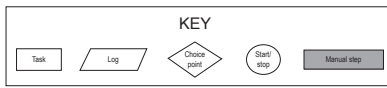


Figure S1, related to Figure 1. Cell movements following pipette navigations into the brain.

(A-B) Target cell displacements in the transverse plane (left) and their magnitude (right), following pipette navigations into the brain. Δx , change in the x coordinate of the target cell centroid, with a positive value corresponding to a cell movement to the right relative to the original location; Δy , change in the y coordinate of the target cell centroid, with a positive value corresponding to a cell movement in the anterior direction relative to the original location. Each circle represents a movement of a single cell, while squares and error bars are mean \pm standard deviation.

(A) Target cell movements following pipette navigation along a linear trajectory parallel to the pipette axis ($n = 25$ cells in 6 anesthetized mice), with the pipette moving from above the brain surface to cortical layer 2/3.

(B) Target cell movements following pipette navigation in the x, y, and z directions ($n = 27$ cells in 17 anesthetized mice), with the pipette moving from a point 20 – 30 μm away from the target cell centroid to a point 10 – 20 μm directly above the target cell centroid.



Setup
 Target cell detection & selection (Fig. 1B(i))
 Pipette tip detection (Fig. 1B(ii))
 Brain penetration (Fig. 1B(iii))
 Closed-loop real-time image-guided pipette positioning (Fig. 1A and Fig. 1B(iv))
 Gigaseal formation (Fig. 1B(v))
 Break-in (Fig. 1B(vi))

Figure S2, related to Figure 1. Step-by-step flowchart, showing the entire imagepatching process.

Dotted lines frame each of the stages of the algorithm; within the dotted line frames, symbols represent task, logging, and choice points, along with text explaining the individual steps and consequences of each decision (see “**KEY**” for definition of symbols). Abbreviations: Z , depth inside the brain, in microns (with more positive Z values indicating deeper positions inside the brain); Z_{cell} , depth of the target cell, X_{cell} , x-coordinate of the target cell centroid at Z_{cell} ; Y_{cell} , y-coordinate of the target cell centroid at Z_{cell} ; x , movement direction along the x-axis of the 4-axis manipulator; y , movement direction along the y-axis of the 4-axis manipulator; z , movement direction along the z-axis of the 4-axis manipulator; d , movement direction along the diagonal axis (i.e., axis parallel to the pipette) of the 4-axis manipulator; $R(Z)$, pipette resistance at depth Z ; N_p , counter for the pipette clearing pressure pulse; N_{cl} , total number of times the closed-loop is run; N_{clmax} , limit on the number of times the closed-loop is run; Z_{cl} , depth at which pipette pressure is lowered to 30 mBar; $R(Z_{cl})$, pipette resistance at Z_{cl} ; $HBM(Z_{cl})$, amount of heartbeat modulation at Z_{cl} ; $R(Z_{seal})$, pipette resistance at the depth at which a gigaseal and the whole-cell state are being achieved, which will vary over time as the algorithm progresses; T_1 , time, in seconds; T_2 , time, in seconds; N_s , total number times a suction pulse is applied for break-in; N_{smax} , limit on the number times a suction pulse is applied for break-in; I_d , mean pixel intensity inside the target cell contour, in the microscope channel corresponding to the pipette dye; I_{dg} , I_d when $R(Z_{seal})$ is higher than 1 G Ω ; I_{db} , I_d when $R(Z_{seal})$ is less than 300 M Ω .

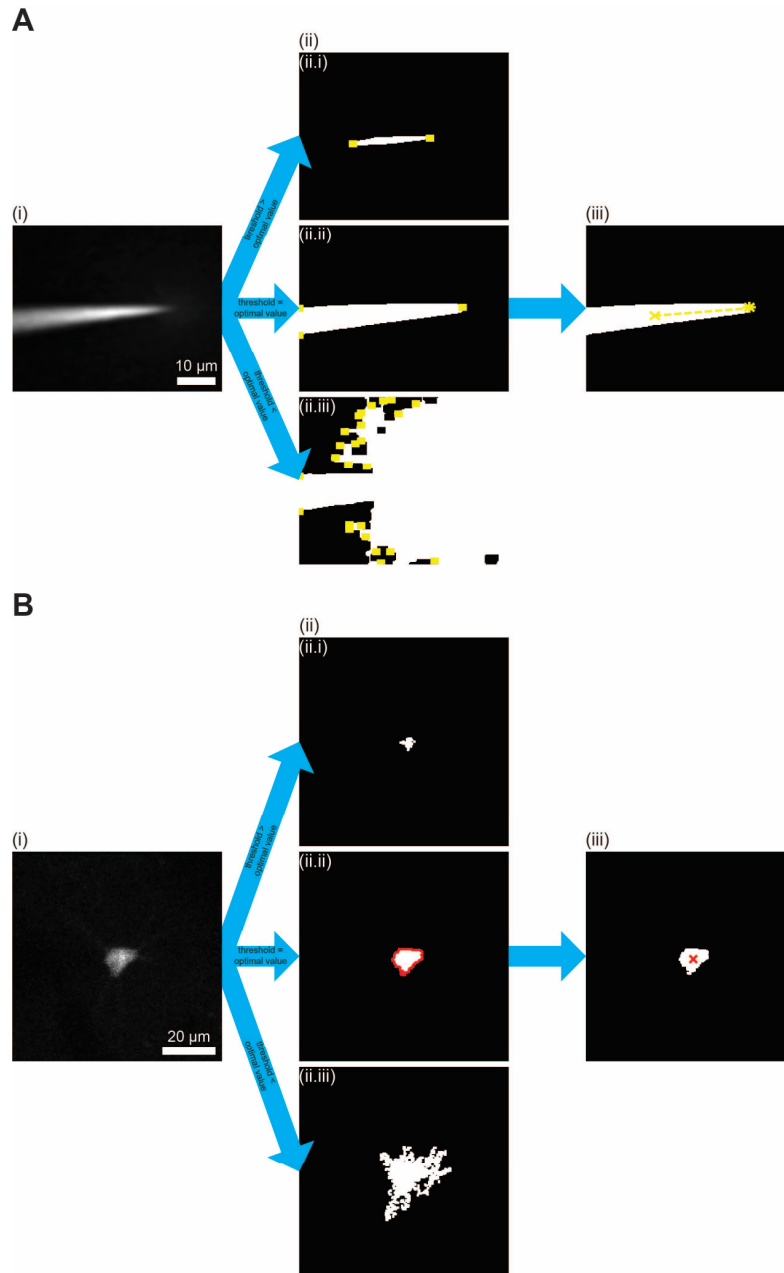


Figure S3, related to Figure 2. 2D image analysis algorithms for detecting pipette tips and cell centroids.

(A) Steps used to detect the tip of a fluorescent dye filled patch pipette from an image focused on the pipette tip. (i) An image of the pipette at the z-coordinate of the pipette tip (i.e., an image focused on the pipette tip) is filtered using a 2D Gaussian filter. (ii) Threshold values corresponding to 5 – 75% of the maximum pixel intensity of the filtered image are applied to the filtered image, and the resulting clusters (white) are subjected to MATLAB’s endpoint detection function (bwmorph function with ‘endpoints’ operation) to identify the endpoints (yellow boxes). Clusters and endpoints resulting from threshold values corresponding to 75% (ii.i), 13% (i.e., optimal threshold value; ii.ii), and 3% (ii.iii) of the filtered image’s maximum pixel intensity are shown as examples. (iii) The cluster resulting from the optimal threshold value is analyzed to locate its

centroid (yellow x) and extrapolate a line from the centroid in the direction of the pipette angle (yellow dotted line). The pixel in the cluster that is closest to the endpoint of the extrapolated line (i.e., endpoint opposite to the centroid) is designated as the pipette tip (yellow star).

(B) Steps used to detect the cell boundary and centroid from each image in a z-stack acquired around a fluorescent cell. (i) An image in a z-stack acquired around a tdTomato-expressing cell is filtered using a 2D Wiener filter. (ii) Threshold values corresponding to 5 – 95% of the maximum pixel intensity of the filtered image are applied to the filtered image, and the resulting clusters (white) are analyzed to determine their areas (i.e., numbers of pixels in the clusters). The cluster whose area is the closest to that of the cell chosen by the user during the target cell detection and selection stage ((ii.ii), white) is further processed to determine its boundary ((ii.ii), red outline). Clusters resulting from threshold values corresponding to 50 (ii.i), 20 (i.e., optimal threshold value; ii.ii), and 3.5% (ii.iii) of the filtered image's maximum pixel intensity are shown as examples. (iii) The cluster obtained by applying the optimal threshold value to the image at the z-coordinate of the cell centroid is processed to yield its centroid (red x), designated as the centroid of the cell.

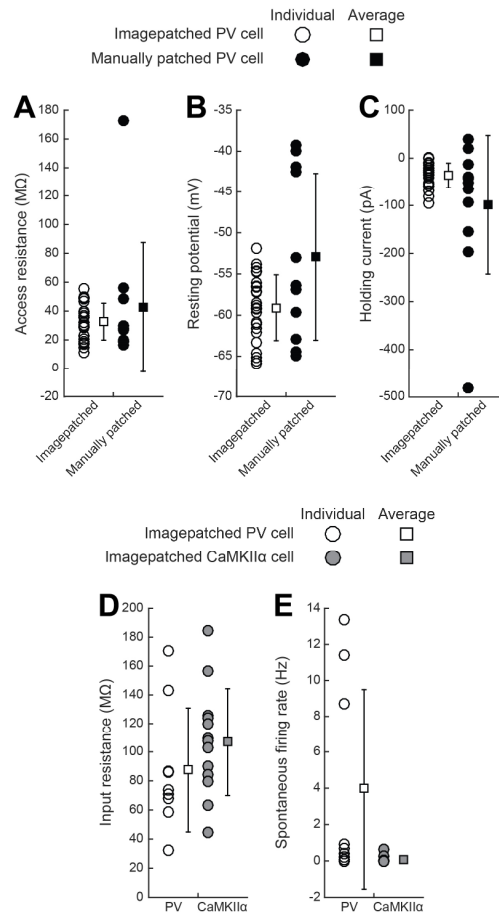


Figure S4, related to Figure 4. Recording quality and electrophysiological properties of imagepatched neurons.

(A-C) Recording quality of imagepatched (white symbols; $n = 24$ cells from 14 mice) vs manually patched (black symbols; $n = 11$ cells from 8 mice) tdTomato-expressing PV-positive interneurons in somatosensory and motor cortices of isoflurane-anesthetized PV-Cre x Ai14 mice. Squares and error bars are mean \pm standard deviation.

(A) Access resistance.

(B) Resting potential.

(C) Holding current.

(D-E) Electrophysiological properties of imagepatched tdTomato-expressing PV-positive neurons (white symbols; 9 cells from 5 PV-Cre x Ai14 mice) and imagepatched tdTomato-expressing CaMKII α -positive neurons (gray symbols; 13 cells from 7 CaMKII α -Cre x Ai14 mice) in somatosensory and motor cortices of isoflurane-anesthetized mice. Squares and error bars are mean \pm standard deviation.

(D) Input resistance.

(E) Spontaneous firing rate.

Failure Modes	PV	CaMKIIα
Pipette Blockage	20.4% (n = 22)	21.5% (n = 14)
Failed Gigaseal Formation	37.0% (n = 40)	43.1% (n = 28)
Loss of Seal During Break-in	16.7% (n = 18)	9.2% (n = 6)
Untargeted Patch	3.7% (n = 4)	6.2% (n = 4)

Table S1, related to Figure 4. Four failure modes of the imagepatcher.

Imagepatching attempts that did not result in successful whole-cell recordings (84 out of 108 attempts targeting PV-positive neurons, from 17 PV-Cre x Ai14 mice; 52 out of 65 attempts targeting CaMKII α -positive neurons, from 10 CaMKII α -Cre x Ai14 mice) can be grouped into 4 failure modes: (i) ‘pipette blockage’ includes imagepatching attempts in which a pipette failed to eject enough dye at its tip or experienced a significant rise in its resistance value after entering the brain or while approaching the target cell; (ii) ‘failed gigaseal formation’ includes imagepatching attempts in which contact between an uncontaminated pipette tip and the target cell membrane, followed by pipette pressure modulation and hyperpolarization, did not result in a gigaseal; (iii) ‘loss of seal during break-in’ includes imagepatching attempts in which application of suction pulses following successful gigaseal formation led to a loss of gigaseal or cell lysis; and (iv) ‘untargeted patch’ includes imagepatching attempts in which an unlabeled cell (i.e., a cell that was not fluorescently tagged), sitting right on top of a targeted cell, was patched instead of the target cell.

Target Cell Depths Below The Brain Surface	Success Rates			
	PV		CaMKII α	
	Gigaseal	Whole-cell	Gigaseal	Whole-cell
≥ 100 and < 200 μm	50.0% (n = 24 out of 48)	29.2% (n = 14 out of 48)	40.0% (n = 14 out of 35)	25.7% (n = 9 out of 35)
≥ 200 and < 300 μm	48.6% (n = 18 out of 37)	27.0% (n = 10 out of 37)	31.3% (n = 5 out of 16)	25.0% (n = 4 out of 16)

Table S2, related to Figure 4. Success rates at different target cell depths, for trials that entered the closed-loop stage of imagepatching.

One unsuccessful attempt targeted a PV-positive cell at a depth below 300 μm and is not included in the table.

PV			CaMKII α		
Number of Labeled Cells in 200 x 200 x 100 μm^3 Volume	Success Rates		Number of Labeled Cells in 200 x 200 x 100 μm^3 Volume	Success Rates	
	Gigaseal	Whole-cell		Gigaseal	Whole-cell
<6	42.1% (n = 8 out of 19)	31.6% (n = 6 out of 19)	<20	40.0% (n = 4 out of 10)	30.0% (n = 3 out of 10)
≥ 6 and <10	57.1% (n = 16 out of 28)	32.1% (n = 9 out of 28)	≥ 20 and <35	30.8% (n = 4 out of 13)	15.4% (n = 2 out of 13)
≥ 10 and <14	33.3% (n = 8 out of 24)	20.8% (n = 5 out of 24)	≥ 35 and <65	47.1% (n = 8 out of 17)	35.3% (n = 6 out of 17)
≥ 14	66.7% (n = 10 out of 15)	26.7% (n = 4 out of 15)	≥ 65	27.3% (n = 3 out of 11)	18.2% (n = 2 out of 11)

Table S3, related to Figure 4. Success rates for different labeling densities of cells around a target cell, for trials that entered the closed-loop stage of imagepatching.

The number of labeled cells around a target cell in a 200 x 200 x 100 μm^3 volume was determined by scaling the number of tdTomato-expressing cells in a z-stack (5 images, 10 μm step size, field of view of 223.5 x 223.5 μm^2) that captured the target cell near the center of its field of view.